High Resolution 3D X-Ray Diffraction Microscopy

Jianwei Miao,[1,*] Tetsuya Ishikawa,[2] Bart Johnson,[1] Erik H. Anderson,[3] Barry Lai,[4] and Keith O. Hodgson[1,5]

[1]*Stanford Synchrotron Radiation Laboratory, Stanford Linear Accelerator Center, Stanford University, Stanford, California 94309-0210*

[2]*SPring-8/RIKEN, 1-1-1 Kouto, Mikazuki, Sayo-gun, Hyogo 679-5148, Japan*

[3]*Center for X-ray Optics, Lawrence Berkeley National Laboratory, Berkeley, California 94720*

[4]*Advanced Photon Source, Argonne National Laboratory, Argonne, Illinois 60439*

[5]*Department of Chemistry, Stanford University, Stanford, California 94305*

(Received 15 April 2002; published 6 August 2002)

We have imaged a 2D buried Ni nanostructure at 8 nm resolution using coherent x-ray diffraction and the oversampling phasing method. By employing a 3D imaging reconstruction algorithm, for the first time we have experimentally determined the 3D structure of a noncrystalline nanostructured material at 50 nm resolution. The 2D and 3D imaging resolution is currently limited by the exposure time and the computing power, while the ultimate resolution is limited by the x-ray wavelengths. We believe these results pave the way for the development of atomic resolution 3D x-ray diffraction microscopy.

DOI: 10.1103/PhysRevLett.89.088303 PACS numbers: 81.07.Bc, 42.30.Rx, 42.30.Wb, 61.10.Dp

The development of imaging techniques has played a crucial role in understanding the microscopic world. One of the recent innovations, the invention of the tunneling microscope in 1982 [1], spawned a wealth of development of probe microscopes which have found wide ranging applications. These forms of microscopy, however, are primarily sensitive to surface information. By employing innovative aberration-correction techniques, transmission electron microscopes can probe the structure of thin film samples at atomic resolution, but the samples have to be thinner than $\sim$50 nm to avoid the multiple scattering effects [2]. To nondestructively probe thicker samples (>0.5 μm), x rays are more ideal due to their longer penetration length compared to that of electrons. However, x rays are more difficult to focus than electrons. By using Fresnel zone plates, the smallest x-ray focal spot currently achievable is around 30 nm for soft x rays [3] and 150 nm for hard x rays [4]. To achieve better resolution, diffraction methodology such as x-ray crystallography, with the resolution typically limited by the quality of sample diffraction, is the method of choice. X-ray crystallography has had a tremendous impact in materials sciences, chemistry, structural biology, and other areas, but is applicable only to structures with periodic repeats (most typically crystals). Many samples, however, such as amorphous and disordered materials including polymers, strains and defects in crystals, and some inorganic nanostructures, cannot be accessed by this approach. In biology, structures such as whole cells, subcellular structures, and viruses are very often noncrystalline or nonrepetitive. At the molecular level, somewhere around 20%–40% of all of the protein molecules including most of the important membrane proteins are difficult to crystallize and are, hence, not currently accessible by x-ray crystallography.

One form of microscopy, the combination of the coherent x-ray diffraction with the oversampling phasing method [5,6], has the potential to overcome these limitations (another potential approach is to use the transport of intensity method [7]). When a finite specimen is illuminated by coherent x rays, the weakly scattered x-ray photons form a continuous diffraction pattern in the far field. This continuous pattern can be sampled at spacing finer than the Nyquist frequency (i.e., the inverse of the size of the specimen), which corresponds to surrounding the electron density of the specimen with a no-density region [8]. The higher the sampling frequency, the larger the no-density region. When the no-density region is larger than the electron density region, the phase information is, in principle, available from the diffraction pattern itself and can be directly retrieved by using an iterative algorithm [8,9]. The first demonstration experiment of this form of microscopy was carried out by using coherent soft x rays in 1999 [10]. More recently, it has been extended to image the shapes of nanocrystals by using hard x rays [11,12]. The potential applications of this approach to imaging magnetic materials [13,14], nanocrystals [15], and biomolecules [16] have also been pursued. However, the experiments that have been carried out thus far have been limited to imaging 2D samples, and the highest resolution achieved until now is around 70 nm [10,11] . In this Letter, by using coherent x rays with a wavelength of 2 Å, we report the successful imaging of a 2D buried structure at 8 nm resolution. For the first time, we also report the reconstruction of the 3D structure of a noncrystalline sample at 50 nm resolution from a series of diffraction pattern projections.

The oversampling phasing method is strongly correlated to the coherence of the incident x rays. Since oversampling a diffraction pattern corresponds to generating a no-density region surrounding the electron density of the specimen, the coherence length of the incident x rays must be longer than or equal to the overall size of the electron density and the no-density region. Typically, the higher the oversampling degree, the higher the required degree of coherence.

The required spatial and temporal coherence for the oversampling method are expressed as $\Delta\theta \leq \lambda/2Oa$ and $\lambda/\Delta\lambda \geq Oa/d$, where $\Delta\theta$ is the divergence or convergence angle of the incident x rays, λ is the x-ray wavelength, O is the oversampling degree defined as the ratio of the radius of the electron density and the no-density region to the radius of the electron density region, a the sample size, and d the desired resolution.

The sample, fabricated by electron beam lithography, consists of two single-layered Ni patterns (each with a size of $2.5 \times 2 \times 0.1$ μm) rotated relatively 65° to each other in-plane and separated by a distance of 1 μm. The sample is supported by a thin silicon nitride membrane window. Figure 1(a) shows a scanning electron microscopy (SEM) image of the sample. Because of the 1 μm separation of the two layers, the SEM image shows the pattern in the top layer, and the pattern in the bottom layer is visible only as a soft blur. The experiments were carried out on an undulator beam line at SPring-8 with a wavelength of 2 Å. To achieve the desired coherence for the imaging experiments, a 150 μm horizontal slit was placed at a distance of 27 m upstream of the sample for obtaining the spatial coherence of $\Delta\theta < 1.5 \times 10^{-5}$ rad and a Si (1,1,1) double crystal for temporal coherence of $\lambda/\Delta\lambda \sim 7500$ [17]. Two-dimensional patterns were recorded from the sample. To improve the resolution, a CCD detector was shifted in both X and Y directions to record a set of diffraction patterns at different resolutions. These patterns were then tiled together to form a high-resolution diffraction pattern. Figure 1(b) shows a diffraction pattern with 1760×1760 pixels and a resolution of 8 nm at the edge. The total exposure time of the diffraction pattern is about 45 min using unfocused x rays from the undulator beam line. Since a beam stop is used to block the direct beam, the diffraction pattern has an area of missing data at the center with a size of 60×60 pixels, which was filled in by a patch of the intensities calculated from the magnitude of the Fourier transform of an x-ray microscopy image of the sample [18]. To convert the diffraction pattern to a high-resolution image, a reconstruction was carried out by using a random phase set as an initial input and a 2.8×2.6 μm square as the finite support (which is used to separate the electron density and no-density regions). Figure 1(c) shows the reconstructed image in which a line scan through an edge indicates a resolution of 8 nm. The top and bottom layered patterns are clearly seen as overlapped in this 2D image projection, and the variation of the electron density on the nanometer scale is also visible. Five more reconstructions with different random initial phase sets were done and the reconstructed images consistently and faithfully reproduced the original sample pattern. Because of the longer penetration length of hard x rays than of electrons, it can be seen that this form of microscopy can image much thicker specimens at very high resolution. This is probably beyond the capability of both scanning probe microscopy and transmission electron microscopy.

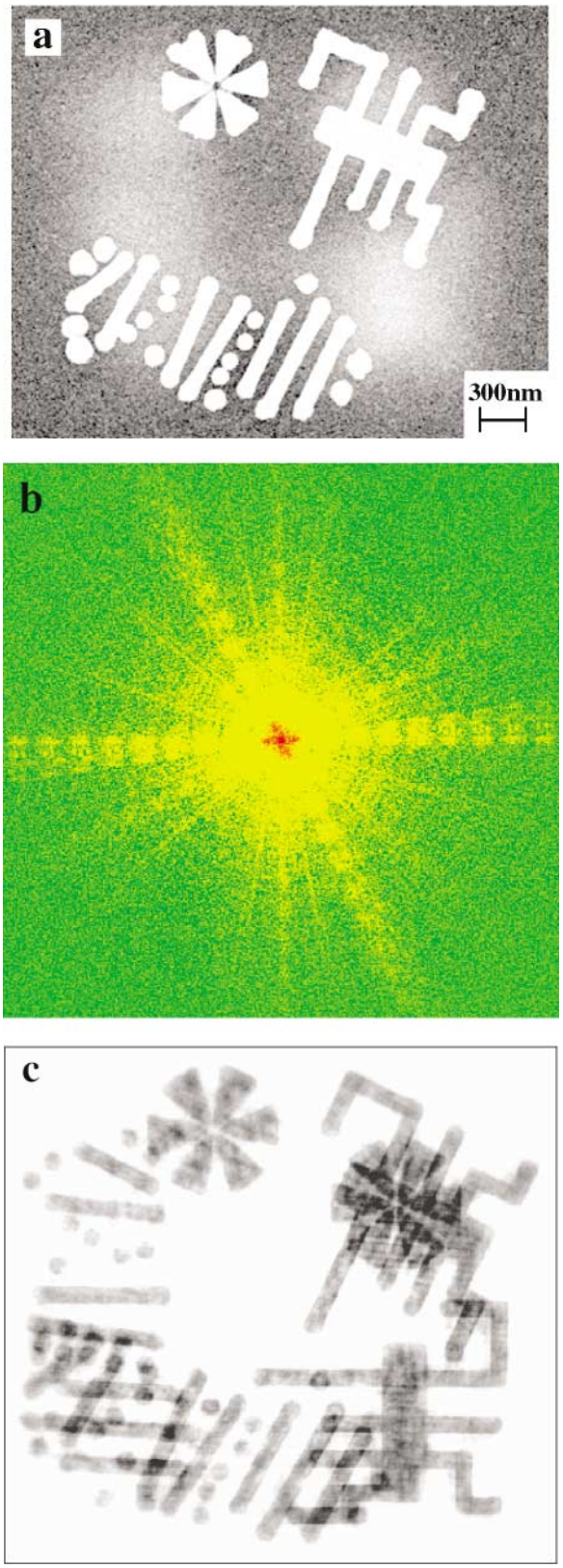

FIG. 1 (color). (a) A SEM image of a Ni sample with buried structures. (b) A high-resolution diffraction pattern (a 1760×1760 pixel array) recorded from the sample. (c) A high-resolution image reconstructed from (b).

We have also developed an algorithm for the reconstruction of 3D images from a limited number of 2D diffraction pattern projections. The series of 2D diffraction patterns, which have a common rotation axis defined as the Z axis, is first mapped onto a 3D array based on an approach illustrated in Fig. 2 (where only one quarter of the array is displayed). For simplicity, each 2D diffraction pattern is assumed to lie on a plane, which is a good approximation when the resolution is not near the atomic level. At very high resolution, each diffraction pattern actually lies on the surface of the curved sphere (the Ewald sphere), but the mechanism discussed here is, in principle, the same. $G(i, j)$ represents, for a given z coordinate, the diffraction intensity in voxel (i, j) as mapped onto the 3D array, where a voxel is the smallest volume element in the 3D array, and $F(\theta_m, n)$ the value of pixel (θ_m, n) in the diffraction pattern with the rotation angle of θ_m. We suppress the z coordinate because formulas are the same for all z. $G(i, j)$ is calculated by

$$G(i,j) = \begin{cases} \dfrac{\sum_{\theta_m,n} w(i,j,\theta_m,n) F(\theta_m,n)}{\sum_{\theta_m,n} w(i,j,\theta_m,n)} & \text{when } \sum_{\theta_m,n} w(i,j,\theta_m,n) \geq 0.5 \\ -1 & \text{when } \sum_{\theta_m,n} w(i,j,\theta_m,n) < 0.5, \end{cases} \quad (1)$$

where $w(i, j, \theta_m, n)$, the volume overlap factor, is equal to 1 when voxel (i, j) and pixel (θ_m, n) are completely overlapped, and 0 when they do not overlap. Here, $G(i, j) = -1$ is used to represent the value of that voxel undefined. In Fig. 2, voxel (i, j) overlaps with four pixels in which the overlapped regions are in colors. Since the total overlapped volume is larger than 0.5 in this case, $G(i, j)$ is calculated from the values of the four colored regions. When the number of the diffraction pattern projections is large enough so that all of the voxels in the 3D array overlap with the pixels in the diffraction patterns, the 3D array can be completely mapped out and there are no undefined voxels. With a limited number of projections, a 3D array can also be calculated in which a number of the voxels are undefined. In each case, the 3D array can be reconstructed by using the following iterative algorithm without the need of interpolation. By combining the measured 3D magnitude (i.e., the square root of the 3D array assembled from the diffraction pattern intensity) with a 3D random phase set, a 3D Fourier transform is calculated. The 3D inverse fast Fourier transform (FFT) is applied to obtain a 3D electron density map. Based on the oversampling degree of the diffraction pattern, a box is defined as the finite support. Outside the finite support, the electron density is gradually pushed close to zero. Inside the finite support, the positive electron density remains unchanged and the negative electron density is pushed to zero. By applying FFT on the new 3D electron density map, a new 3D Fourier transform is obtained. The magnitude of the new Fourier transform is then replaced with the measured 3D magnitude. If the measured 3D magnitude has a number of undefined voxels, only the values of the defined voxels are replaced, and the value of those undefined voxels in the magnitude of the new Fourier transform are kept unchanged. Another 3D Fourier transform is thus obtained. This represents one iteration of the algorithm. Usually, after a few hundred to a few thousand iterations, the correct phases can be retrieved.

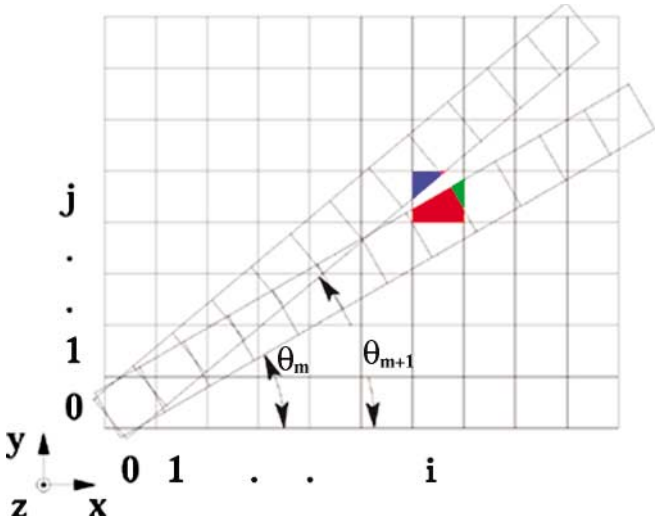

FIG. 2 (color). Schematic layout of the mapping of a 3D array from a series of diffraction pattern projections. The value of voxel (i, j) in this case is calculated from the values of four pixels, part of which are shown in different colors.

By employing this algorithm, a 3D reconstruction has been carried out using a series of thirty-one 2D diffraction patterns recorded from the sample with the rotation angles ranging from $-75°$ to $75°$ in $5°$ increments. The exposure time of each diffraction pattern was around 20 min, and the resolution at the edge is about 28 nm. All the diffraction patterns have a missing data area at the center due to the beam stop except for the one corresponding to the rotation angle of $0°$, in which the missing data was filled in by the intensities calculated from a soft-x-ray microscopy image. Since these diffraction patterns have a common rotation axis, the intensity points on the common axis were used to scale and align the diffraction patterns. The 2D diffraction patterns are then assembled to a 3D diffraction pattern based on Eq. (1). The 3D diffraction pattern, with many undefined voxels, has a resolution of 50 nm at the edge. By using a 3D random phase set as an initial input and a box of $2.8 \times 2.6 \times 1.2$ μm as the finite support, the structure of the 3D specimen at 50 nm is successfully reconstructed. The reconstructed pattern in the top and bottom layer is

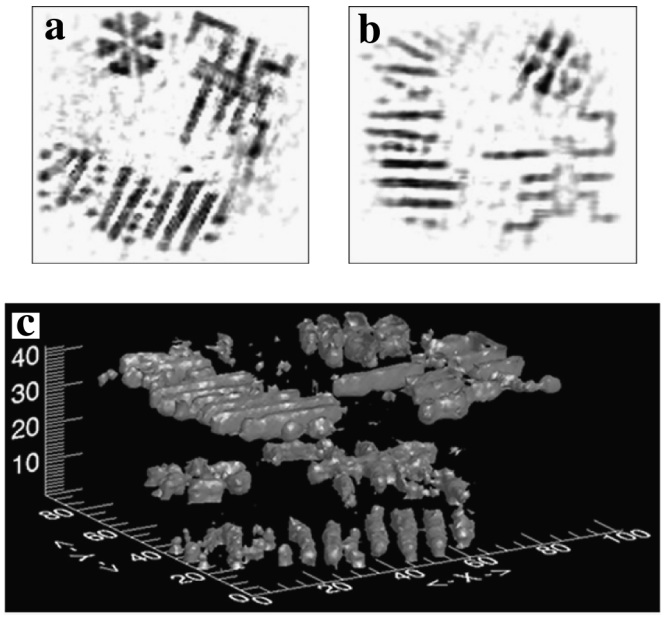

FIG. 3. The reconstruction of a 3D nanostructured material at 50 nm resolution. (a), (b) The reconstructed top and bottom layered pattern. (c) The reconstructed 3D structure displayed in isosurface rendering.

shown in Figs. 3(a) and 3(b), respectively. The two patterns are rotated relatively 65° to each other as in the original sample. Figure 3(c) shows a 3D isosurface rendering of the reconstructed image. The finest division in the z axis corresponds to 25 nm and the distance between two patterns is about 1 μm, which is consistent with the known characteristics of the sample.

We believe this form of microscopy will have wide applications in both materials and biology. For materials science samples, which are less sensitive to radiation damage, this form of microscopy can, in principle, achieve atomic resolution in three dimensions by either having a long exposure time or using higher flux coherent x-ray sources. In biology, this form of microscopy can be applied to image the 3D structures of whole cells, cellular organelles, and supramolecular structures at high resolution, while the resolution will be mainly limited by radiation damage to the specimens [19]. To alleviate the radiation damage problem, biological samples need to be frozen at the temperature of liquid nitrogen [20]. With the prospects of the x-ray free electron lasers (X-FEL) [21] providing ultrashort and extremely intense pulses, the radiation damage problem could possibly be circumvented by recording the diffraction pattern from a single biomolecule before it is destroyed by a single shot [22]. In combination of a simulated X-FEL with this form of microscopy, it has been shown that a 3D diffraction pattern calculated from 10^6 identical rubisco molecules can be successfully converted to a high quality electron density map with a resolution of 2.5 Å [16].

We thank D. Sayre, J. Kirz, and J. C. H. Spence for many stimulating discussions; Y. Nishino, Y. Kohmura, K. Tamasaku, M. Yabashi, Z. Cai, and I. McNulty for the help of data acquisition; P. Pianetta for help in designing the apparatus; and G. Schneider and G. Denbeaux for imaging the specimens by using the soft-x-ray microscope at the Advanced Light Source. This work was supported by the U.S. Department of Energy, Office of Basic Energy Sciences. Additional support was provided by the U.S. DOE Office of Biological and Environmental Research and the National Institutes of Health. Use of the RIKEN beam line (BL29XUL) at SPring-8 was supported by RIKEN.

*Corresponding author.
Email address: miao@ssrl.slac.stanford.edu

[1] G. Binnig, H. Rohrer, C. Gerber, and E. Weibel, Phys. Rev. Lett. **49**, 57 (1982).
[2] J. C. H. Spence, *Experimental High-Resolution Electron Microscopy* (Oxford University Press, New York, 1988).
[3] S. Spector, C. Jacobsen, and D. Tennant, J. Vac. Sci. Technol. B **15**, 2872 (1997).
[4] W. Yun *et al.*, Rev. Sci. Instrum. **70**, 2238 (1999).
[5] D. Sayre, in *Imaging Processes and Coherence in Physics*, Springer Lecture Notes in Physics, edited by M. Schlenker *et al.* (Springer-Verlag, Berlin, 1980), Vol. 112, pp. 229–235.
[6] J. Miao, J. Kirz, and D. Sayre, Acta Crystallogr. Sect. D **56**, 1312 (2000).
[7] K. A. Nugent *et al.*, Phys. Rev. Lett. **77**, 2961 (1996).
[8] J. Miao, D. Sayre, and H. N. Chapman, J. Opt. Soc. Am. A **15**, 1662 (1998).
[9] J. R. Fienup, Appl. Opt. **21**, 2758 (1982).
[10] J. Miao, P. Charalambous, J. Kirz, and D. Sayre, Nature (London) **4000**, 342 (1999).
[11] I. K. Roninson *et al.*, Phys. Rev. Lett. **87**, 195505 (2001).
[12] I. A. Vartanyants and I. I. K. Robinson, J. Phys. Condens. Matter (to be published).
[13] J. Stöhr (private communication).
[14] T. O. Mentes, C. Sánchez-Hanke, and C. C. Kao, J. Synchrotron Radiat. **9**, 90 (2002).
[15] J. Miao and D. Sayre, Acta Crystallogr. Sect. A **56**, 596 (2001).
[16] J. Miao, K. O. Hodgson, and D. Sayre, Proc. Natl. Acad. Sci. U.S.A. **98**, 6641 (2001).
[17] K. Tamasaku *et al.*, Nucl. Instrum. Methods Phys. Res., Sect. A **467–468**, 686 (2001).
[18] J. Kirz, C. Jacobsen, and M. Howells, Q. Rev. Biophys. **28**, 33 (1995).
[19] R. Henderson, Q. Rev. Biophys. **28**, 171 (1995).
[20] J. Maser *et al.*, J. Microsc. **197**, 68 (2000).
[21] Web address: www-ssrl.slac.stanford.edu/lcls.
[22] R. Neutze *et al.*, Nature (London) **406**, 752 (2000).